Simulating the Behavior of Restrained Steel Beams to Flame Impingement from Localized-Fires

Chao Zhang[a,b,*], Guo-Qiang Li[c,**], Asif Usmani[d]

[a] *College of Civil Engineering, Tongji University, 1239 Siping Road, Shanghai 200092, China*
[b] *National Institute of Standards and Technology, National Fire Research Laboratory, Fire Research Division, Gaithersburg, MD 20899-1070, USA*
[c] *State Key Laboratory for Disaster Reduction in Civil Engineering, Tongji University, 1239 Siping Road, Shanghai 200092, China*
[d] *School of Engineering, Edinburgh University, Edinburgh EH9 3JN, UK*

Abstract

Steel structures may be exposed to localized heating by a fire source nearby. Flame impingement from localized fire may lead to high temperatures in the exposed steel members, which may lead to structural failure. This paper numerically investigates the thermal and mechanical behaviors of restrained steel beams exposed to flame impingement from localized fires. Four steel beams with different dimensions and restraints were considered. Both developing and steady burning fires were investigated. The standard ISO834 fire was also used for comparison. The study finds that the temperature distributions within the steel beams subjected to flame impingement are highly non-uniform both across and along the beams. Along the beam length, the temperatures near the fire source may be hundreds of degrees higher than those far from the fire source. Due to different temperature distribution, the deformation mode for restrained steel beam subjected to flame impingement may be significantly different from that of a beam subjected to the standard ISO834 fire. The failure temperatures for restrained steel beams subjected to localized fires may be higher or lower than those for restrained beams subjected to the standard ISO834 fire. Reliance on the standard fire may lead to an unconservative design if the potential real fires are localized fires.

*Currently Guest Scientist at NIST. E-mail address: chao.zhang@nist.gov or 08_chao_zhang@tongji.edu.cn(C. Zhang).

**E-mail address: gqli@tongji.edu.cn(G.Q. Li)

Keywords: Restrained steel beam; Flame impingement from localized fire; Thermal and mechanical behavior; Numerical investigation

1. Introduction

In the past two decades, many researchers have investigated the behavior of steel beams exposed to fire [1, 2, 3, 4, 5, 6, 7, 8, 9, 10]. Liu et al. [1] experimentally investigated the role of the connections and axial restraint in affecting the fire resistance of a steel beam. In their experiments, the furnace was programmed to follow the ISO834 standard temperature-time curves. Li and Guo [2] tested the behavior of restrained steel beams subjected to a natural fire. In the test, an arbitrary temperature-time curve which included both heating and cooling phases was used to represent the natural fire. Vila Real et al. [3] conducted a validation test on the lateral-torsional buckling resistance of unrestrained steel I beams subjected to fire. In the test, the thermal action on a simply supported beam was changed from room temperature up to 600 ^{o}C. In [1, 2, 3], all the specimens in the furnace were heated uniformly such that the longitudinal temperature gradients were negligible. In [1, 2], the upper flanges of the tested beams were protected with fireproofing materials to consider the heat-sink effect resulting from concrete slabs on the steel beams in real building construction. As a result, the transverse temperature gradients in the specimens were very large (in both tests [1, 2], the maximum temperature differences between the upper and lower flange were on the order of several hundreds of degrees). In [3], the beam was unprotected so that the transverse temperature gradient was negligible. Recently, the effect of transverse thermal gradient on the behavior of steel beam-columns exposed to fire was experimentally investigated by Dwaikat et al. [4]. In their experiment, both ASTM E119 standard fire and a design fire were considered. The design fire included a growth phase simulating the ASTM E119 standard fire for about 90 min and then underwent a rapid cooling phase. The specimens with uniform insulation were exposed to fire from four sides, and the insulation on some specimens was removed in specific locations to cause thermal gradient.

Yin and Wang [5, 6], Li et al. [7], Tan and Huang [8], Bailey et al. [9], Usmani et al. [10], EI-Rimawi et al.[11] and Kodur and Dwaikat [12], on the other hand, have numerically investigated the behavior of steel beams in fire conditions. Among those studies, [5, 6, 7, 8] considered the effects

of non-uniform temperature distributions in their investigations. However, the profiles of those non-uniform temperature distributions (transversely or longitudinally) were arbitrarily assumed and considered to be linear.

The fire conditions used in the studies mentioned above are all designed to represent fully-developed compartment fires or post-flashover fires. In a fully-developed compartment fire, the gas properties within the compartment are approximately uniform because of flashover. Correspondingly, the steel members exposed to compartment fires are uniformly heated on all exposed sides such that the temperature gradients along the length of the members are always negligible and the temperature distributions within the steel sections are approximately uniform (as in steel columns) or varying linearly with depth (as in ceiling steel beams). However, in some spaces such as open car park buildings and large enclosures where fuels are located in specific areas so that horizontal fire spread is not possible, the flashover phenomena (that all exposed fuel surfaces within the compartment burn simultaneously [13]) are unlikely to happen. Localized fires are more appropriate when evaluating the fire safety of structures in such spaces.

The gas properties in a localized fire are highly non-uniform and the temperature distributions in the exposed steel members are longitudinally and transversely nonlinear [14, 15]. Until now, few reports on the behavior of steel beams exposed to localized fires have been issued. Hasemi et al. [16] experimentally studied the heating mechanism of ceiling/beams exposed to localized fires. Based on the test data, a correlation was proposed by Hasemi to calculate the heat flux to the ceiling from flame impingement from localized fires. The correlation has been adopted by the Eurocode EC1 [17]. In SFPE handbook [18], the correlations proposed by Wakamatsu are adopted to calculate the heat fluxes to different parts of steel I beams from localized fires. Recently, Jeffers and Sotelino [19] simulated the thermo-mechanical behavior of a simply supported steel beam exposed to a localized fire by a computationally efficient fiber element approach.

The purpose of this study is to investigate the thermal and structural behaviors of restrained steel beams exposed to localized fires. Correlations recommended by SFPE handbook were used to calculate the heat fluxes to exposed steel I beams. The finite element program ANSYS [1] was used as the

[1]Certain commercial entities, equipment, or materials may be identified in this document in order to describe an experimental procedure or concept adequately. Such identifi-

numerical tool.

2. Modeling localized fire

2.1. Heat release rate

Heat release rate (HRR) is the most import variable in measuring fire severity, which can be calculated by

$$HRR = \dot{m}_f \cdot \triangle H_c \tag{1}$$

where, $\dot{m}_f$ is the mass burning rate of the fuel; and $\triangle H_c$ is the net heat of combustion of the fuel. In ventilation controlled fires (fully-developed compartment fires), the HRRs are alternatively calculated by

$$HRR = \dot{m}_a \cdot \triangle H_{air} \tag{2}$$

where, $\dot{m}_{air}$ is the mass rate of air inflow; and $\triangle H_{air}$ is the heat released per unit mass air consumed. For most common fuels, $\triangle H_{c,air} = 3.03 \pm 0.02$MJ/kg [13].

The HRR of a real fire can be measured by cone calorimetry (see Babrauskas et al. [20]). In design work, the natural fire safety concept (NFSC) is widely used to represent the fire conditions [17, 21]. As shown in Fig.1, the NFSC fire is assumed to be t-square in the growth stage and decay stage begins at the time when 70 percent of design fire load is consumed. The steady fire with a single constant HRR in the whole fire duration time, which is usually considered in fire resistance design [22], is also illustrated in Fig.1.

For an NFSC fire, in the growth stage, the HRR is given by

$$HRR = \alpha t^2 \tag{3}$$

the fire growth time t_g is given by

$$t_g = \sqrt{\frac{HRR_{max}}{\alpha}} \tag{4}$$

---

cation is not intended to imply recommendation or endorsement by the National Institute of Standards and Technology, nor is it intended to imply that the entities, materials, or equipment are necessarily the best available for the purpose.

and the fuel energy consumed during the fire growth stage, Q_g, is

$$Q_g = \int_0^{t_g} \alpha t^2 dt = \frac{\alpha {t_g}^3}{3} \tag{5}$$

where, α is the fire intensity coefficient, taken as 0.00293, 0.0117 and 0.0466 for slow, medium and fast growth fire, respectively.

The duration time of steady burning in an NSFC fire is given by

$$t_s = \frac{0.7 q_f A_f - Q_g}{HRR_{max}} \tag{6}$$

and the duration of the decaying stage is given by

$$t_d = \frac{0.6 q_f A_f}{HRR_{max}} \tag{7}$$

where, q_f and A_f are design fire load density and floor area, respectively; and HRR_{max} is the maximum heat release rate.

The total duration time of an NFSC fire is given by

$$t_f = t_g + t_s + t_d \tag{8}$$

2.2. Flame length

Heskestad's correlation is used by EC1 [17] to calculate the unconfined flame length of a localized fire, which is given by

$$L_f = -1.02D + 0.235\dot{Q}^{2/5} \tag{9}$$

where, D is the diameter of the fire; and $\dot{Q}$ is the HRR of the fire.

The unconfined flame length can also be calculated by[16]

$$\frac{L_f}{D} = 3.5 {Q_D^*}^n \tag{10}$$

where $n = 2/5$ for $Q_D^* \geq 1.0$ and $n = 2/3$ for $Q_D^* < 1.0$. Q_D^* is a non-dimensional HRR given by

$$Q_D^* = \frac{\dot{Q}}{\rho_\infty c_p T_\infty \sqrt{g} D^{5/2}} \tag{11}$$

where, ρ_∞, c_p and T_∞ are density, specific heat and temperature of gas at ambient temperature; and g is the gravitational acceleration.

For localized fires beneath an unconfined ceiling, the horizontal flame length, defined as the distance between the flame tip and the fire centerline, is given by [18]

$$\frac{L_C + H_C}{H_C} = 2.90 {Q^*_{H_C}}^{1/3} \tag{12}$$

The horizontal flame lengths along the lower and upper flanges of I-beams mounted to a ceiling are given by [18]

$$\frac{L_B + H_B}{H_B} = 2.3 {Q^*_{H_B}}^{0.3} \tag{13}$$

and

$$\frac{L_C + H_C}{H_C} = 2.9 {Q^*_{H_C}}^{0.4} \tag{14}$$

where $Q^*_{H_C}$ and $Q^*_{H_B}$ are defined as in Eq.11 with D is replaced by H_C and H_B, respectively. H_C and H_B are the distances between the fire and the ceiling, and the fire and the lower flange of the beam, respectively.

2.3. Heat flux from localized fire

Hasemi et al. [16, 23, 24] conducted a series of fire tests to investigate the heating mechanisms of building components exposed to localized fires. A flat ceiling with and without a steel I beam beneath it was located at different distances above burners using propane gas fuel. Steady fires were considered in the tests. The HRRs from the fire source ranged from 90 kW to 900 kW in the ceiling/beam tests, and 80 kW to 750 kW in the ceiling tests. Heat flux gauges were used to measure the incident heat flux along the ceiling/beam at different distances away from the fire centerline. A detailed description of the tests is given in [23, 24].

In EC1 [17], the heat flux received by the ceiling exposed to flame impingement from localized fires is given by

$$\dot{q}_{in} = 100 \qquad (y_C \leq 0.30) \tag{15a}$$

$$\dot{q}_{in} = 136.3 - 121 y_C \quad (0.30 < y_C \leq 1.00) \tag{15b}$$

$$\dot{q}_{in} = 15 y_C^{-3.7} \qquad (y_C \geq 1.00) \tag{15c}$$

where $\dot{q}_{in}$ is the incident heat flux in kW; and y_C is a non-dimensional parameter, defined by

$$y_C = \frac{r + H_C + z_0}{L_C + H_C + z_0} \tag{16}$$

in which, z_0 is the vertical position of the virtual heat source, obtained from

$$\frac{z_0}{D} = 2.4(1 - {Q_D^*}^{2/5}) \qquad (Q_D^* \geq 1.0) \tag{17a}$$

$$\frac{z_0}{D} = 2.4({Q_D^*}^{2/5} - {Q_D^*}^{2/3}) \quad (Q_D^* < 1.0) \tag{17b}$$

In the SFPE handbook [18], an alternative correlation proposed by Wakamatsu is presented for calculating the heat flux received by the ceiling, $\dot{q}_{in}$, and is given by

$$\dot{q}_{in} = 518.8e^{-3.7y_C} \tag{18}$$

The heat fluxes incident onto different parts of an I-beam mounted beneath a ceiling can be calculated by the following correlations [18]: the heat flux to the downward face of the lower flange is

$$\dot{q}_{in} = 518.8e^{-3.7y_B} \tag{19}$$

the heat flux to the upward face of the lower flange and the web is

$$\dot{q}_{in} = 148.1e^{-2.75y_C} \tag{20}$$

and the heat flux to the downward face of the upper flange is

$$\dot{q}_{in} = 100.5e^{-2.85y_C} \tag{21}$$

where y_B is defined the same as in Eq.16 with the subscript 'C' is replaced by 'B'.

Myllymaki and Kokkala [18, 25] measured heat fluxes onto I-beams exposed to fires as large as 3.9 MW. They found that for fires over 2.0 MW, the correlations suggested by Wakamatsu for the upward face of the lower flange, web, and downward face of the upper flange underestimate the heat flux to these areas on the I-beam. For these large fires, the I-beam becomes completely engulfed in the fire. As a result, heat fluxes on all parts of the I-beam follow the correlation suggested for the downward face of the lower flange provided in Eq.19.

3. Numerical study

3.1. Numerical tool

The finite element program ANSYS was used as the numerical tool. ANSYS can predict the transient, nonlinear thermal/structural behaviors of various structures under fire conditions if the material properties are provided, as validated by previous studies [21, 26, 27].

3.2. Basic elements

3.2.1. SHELL131-3D layered thermal shell

In the following studies, SHELL131 is used to model the thermal behavior of steel beams in fire conditions. SHELL131 is a 3D layered shell element having in-plane and through-thickness thermal conduction capability. It has 4 nodes with up to 32 temperature degrees of freedom at each node. The element is applicable to a 3D, steady-state or transient thermal analysis. SHELL131 generates temperatures that can be passed to structural shell elements (such as SHELL181) for structural analysis.

The ability of SHELL131 to solve the transient, nonlinear heat transfer problem was verified using an example in Holman's heat transfer book [28]. The problem involves the heating of a 30 mm ceramic wall exposed to a radiation source on one side at 1000 ^{o}C, and to room air at 20 ^{o}C with a radiation surrounding temperature of 20 ^{o}C on the other side. Properties of the ceramic are $k = 3.0$ W/mK, $\rho = 1600$ kg/m^3, and $c = 800$ J/kgK. The emissivity is taken as 0.8. The convection heat transfer coefficient from the heated side of the plate is calculated by $h = 1.92\triangle T^{1/4}$. In [28], the problem was solved by finite difference method (FDM). In a previous work [27], the problem was solved using ANSYS with 2D thermal solid element PLANE55 and thermal surface element SURF151. Fig.2 shows excellent agreement among the results of wall temperatures predicted by the various methods.

3.2.2. SHELL181-finite strain shell

SHELL181 was adopted to model the structural behavior of steel beams in fire. SHELL181 is suitable for analyzing thin to moderately-thick shell structures. It is a 4-node element with six degrees of freedom at each node: translations in the x, y, and z direction, and rotations about the x, y, and z axes. SHELL181 is well-suited for linear, large rotation, and/or large strain nonlinear applications. Change in shell thickness is accounted for in nonlinear analysis.

Ding et al. [29] used SHELL181 to model tests of the fire resistance of fire-resistant steel members. In this paper, the use of SHELL181 to predict the structural behaviors of steel beams in fire was validated using test data from Li and Guo [2] and Liu et al. [1].

Test on specimen 1 in [2] was considered. The tested beam had a cross section H250×250×8×12 and a clear span length of 4500 mm. Two concentrated loads were applied symmetrically to the restrained beam by two jacks. The distance between these two point loads was 1500 mm. The load ratio

(LR) of the restrained beam at room temperature was 0.7. LR was defined as the ratio of the applying moment to the moment capacity of the beam section calculated by design codes. Fig.3 shows the FE structural model of the restrained steel I beam. The steel beam was modeled using SHELL181, and the restraints at the beam ends were modeled using spring-damper element COMBIN14. As shown in Fig.3(b), an axial spring and a rotational spring located at mid-height of the beam end section are used to provide axial and rotational restraints, respectively. The axial stiffness provided is $k_a = 39.54$ kN/mm and the rotational stiffness is $k_r = 1.09 \times 10^8$ Nm/rad. The high temperature material model for structural steel reported in [30] was used in the numerical model. Figs. 4, 5 and 6 show good agreement between the numerical results and test data. The discrepancy between the numerical and measured results could be due to the fact that the stress-strain model in [30] cannot model high temperature creep successfully [12].

Test numbered "FUR15" in [1] was considered. The tested beam had a cross section 178×102×19UB and a clear span length of 2000 mm. Two symmetrical concentrated loads were applied. The distance between these two point loads was 800 mm. The LR of the restrained beam at room temperature was 0.5. End-plate beam-to-column connections were used. The axial stiffness provided is $k_a = 8$ kN/mm and the rotational stiffness is $k_r = 1.4 \times 10^5$ Nm/rad. Figs. 7 and 8 show good agreement between the numerical results and test data.

3.3. FE model and investigated cases

In our investigation, restrained ceiling beams under uniform load subject to flame impingement from localized fires were considered. Table 1 gives characteristics of the investigated cases. In the table, 'R' and 'A' correspond to rotational and axial restraints, respectively. Four beams with different dimensions and restraints were considered. Beam B1 was the above tested beam in [1], and beam B3 was the above tested beam in [2] without ribs. Beam B2 was similar to beam B1 with axial restraint only and B4 was similar to beam B3 with axial restraint only. The LRs for B1 and B2 were 0.5, and for B3 and B4 were 0.7. The ceiling height was 2 m. The fire source was located at the floor and just below the center of the beams. Medium NFSC and steady fires were considered. The maximum heat release rates for those two fires were equal and taken as 1.6 MW. The ISO834 standard fire was also considered for comparison. The fire duration was taken as 1 h. In all cases,

the beams were unprotected and three-sides exposed. The upward surfaces of the beam upper flanges were assumed to be adiabatic.

4. Results and discussions

4.1. Steel temperature distribution

Fig. 9 shows results for the temperature of a steel beam subjected to the NFSC fire. The temperature distributions within steel beam are highly non-uniform both transversely and longitudinally, and the location of the maximum temperature changes with time. At the very beginning of the developing phase, the maximum temperature is located at the lower flange, as shown in Fig. 9a; then, the maximum temperature moves to the web and stays within the web during the later developing and steady burning phases, as shown in Fig. 9b and Fig. 9c; during the decay phase, the maximum temperature first moves from the web to the lower flange, then from the lower flange to the upper flange, as shown in Fig. 9d and Fig. 9e.

Fig. 10 shows results at $t = 300$s and $t = 3000$s for the temperature of a steel beam subjected to the steady fire. The temperature distributions within the steel beam are also highly non-uniform both transversely and longitudinally. During the entire heating phase, the maximum temperature remains within the web.

Fig. 11 shows results for the temperature of a steel beam subjected to the the ISO834 fire. The temperature distribution within the steel beam section is nonlinear. During the entire heating phase, the maximum temperature remains within the web. In simulations using the ISO834 fire, uniform heating conditions along the beam length were assumed; therefore, the steel temperatures are longitudinally uniform, as shown in Fig. 11.

4.2. Structural response

Fig. 12a and 12b show the results of deflection and reaction force, respectively, for the restrained steel beam B1 subjected to different fires. In standard fire test [31], a load-bearing element is definitely failed when either its deflection reaches $L/20$ (for horizontal members) or when it collapses (for vertical members). Here, L is the clear span of the specimen. In our investigation, the failure temperature of restrained beams is defined as the maximum steel temperature when the restrained beams either reach the above deflection limit or buckle. In Fig. 12a, values for the failure temperature are

also presented. Fig. 12b shows that the restrained beam B1 buckles in all investigated fires.

Fig. 13a and 13b show the results of deflection and reaction force, respectively, for the restrained steel beam B2 subjected to different fires. Beam B2 buckles in the NFSC fire. In the steady and ISO834 fires, beam B2 fails when its mid-span deflection reaches $2000/20 = 100$ mm.

Fig. 14a and 14b show the results of deflection and reaction force, respectively, for the restrained steel beam B3 subjected to different fires. Beam B3 buckles in both the NFSC and steady fires. In the ISO834 fire, beam B2 fails when its mid-span deflection reaches $4500/20 = 225$ mm.

Fig. 15a and 15b show the results of deflection and reaction force, respectively, for the restrained steel beam B4 subjected to different fires. Beam B4 buckles in both the NFSC and steady fires. In the ISO834 fire, beam B2 fails when its mid-span deflection reaches $4500/20 = 225$ mm.

The failure modes and failure temperatures (marked as T_{fail}) are summarized in Table 1. Beams in the NFSC fire buckle in all cases; and beams in the steady and ISO834 fires buckle in some cases. For beams B1, B2 and B3, the failure temperatures in the ISO834 fire are lower than those in either the NFSC or steady fire; but for beam B4, the failure temperature in ISO834 fire is higher than that in both the NFSC and steady fires (T_{fail} in ISO834 fire is 514 ^{o}C and 13 % higher than that in the NFSC fire). Generally, the failure temperatures in the NFSC are lower than those in the steady fire.

4.3. Discussions

For steel beams subjected to flame impingement from localized fires, the steel temperatures just above the fire source may be hundreds of degrees higher than those far from the fire source, as shown in Figs. 9 and 10. Due to the nonlinear longitudinal temperature gradient, the restrained beam in localized fires are more likely to undergo lateral displacements. Fig. 16 shows the results of deformations at the definite failure condition for Beam B4 in the NFSC localized fire. The beam undergoes large deflection with global lateral displacement and significant local deformation in the middle section. By comparison, the same beam undergoes only large deflection when subjected to the standard ISO834 fire, as shown in Fig. 17.

The heating history affects the temperature distribution within the exposed member. Therefore, although the maximum heat release rate for the NFSC and steady localized fires are equal, the same beam exposed to those

two fires might behave differently due to the different temperature distributions as illustrated in cases 2a and 2b.

The temperature distribution within the restrained steel beam affects the beam behavior and its failure temperature.

5. Conclusions

The thermal and mechanical behaviors of restrained steel beams subjected to flame impingement from localized fires have been investigated numerically using ANSYS. Based on the results of this investigation, the following conclusions can be drawn:

- The temperature distributions within a steel beam subjected to flame impingement from localized fire are highly non-uniform both along the beam axis and trhough its depth. Along the beam length, the temperatures near the fire source may be hundreds of degrees higher than those far from the fire source.

- The failure temperature for a restrained steel beam subjected to flame impingement from localized fire may be higher or lower than the same beam subjected to the standard ISO834 fire. In the cases investigated, the failure temperature in a localized fire can be 60 ^{o}C or 13 % lower (In the case the failure temperature in the standard ISO834 fire is 514 ^{o}C).

- The deformation mode for a restrained steel beam subjected to flame impingement from localized fire may be different from that subjected to the standard ISO834 fire.

- The structural fire design based on the standard fire may be unconservative if the potential real fires are localized fires.

- Finally, although not specifically investigated here, it has been noted in previous studies (e.g. [10]) that transverse variation of temperatures (causing through-depth temperature gradients) will produce thermal bowing resulting in increase deflection and reduced axial forces in the beam (under weak rotational restraint). Longitudinal variations of temperatures (in the absence of significant transverse gradients) produce the opposite effect, reduced deflections and increased axial forces (under

strong translational restraint). This general observation is consistent with the findings here.

6. Acknowledgement

The work presented in this paper was originated at Tongji University and completed at NIST. The research work at Tongji was partially supported by the National Natural Science Foundation of China through the contract 51120185001. The support is acknowledged.

Valuable suggestions and review comments from Drs. John L. Gross, Jiann C. Yang and Fahim H. Sadek of NIST in the development of the manuscript are gratefully acknowledged.

[1] T.C.H. Liu, M.K. Fahad, J.M. Davies. Experimental investigation of behavior of axially restrained steel beams in fire. Journal of Constructional Steel Research, 2002;58:1211-30.

[2] G.Q. Li, S.X., Guo. Experiment on restrained steel beams subjected to heating and cooling. Journal of Constructional Steel Research, 2008;64:268-74.

[3] P.M.M. Vila-Real, P.A.G. Piloto, J.-M. Franssen. A new proposal of a simple model for the lateral-torsional buckling of unrestrained steel I beams in case of fire: experimental and numerical validation. Journal of Constructional Steel Research, 2003;59:179-99.

[4] M.M.S. Dwaikat, V.K.R. Kodur, S.E. Quiel, M.E.M. Garlock. Experimental behaviour of steel beam-columns subjected to fire-induced thermal gradient. Journal of Constructional Steel Research, 2011;67:30-38.

[5] Y.Z. Yin, Y.C. Wang. A numerical study of large deflection behavior of restrained steel beams at elevated temperatures. Journal of Constructional Steel Research, 2004;60:1029-47.

[6] Y.Z. Yin, Y.C. Wang. Numerical simulations of the effects of non-uniform temperature distributions on lateral torsional buckling resistance of steel I-beams. Journal of Constructional Steel Research, 2003;59:1009-33.

[7] G.Q. Li, P. J. Wang, S.C. Jiang. Non-linear finite element analysis of axially restrained steel beams at elevated temperatures in fire. Journal of Constructional Steel Research, 2007;63:1175-83.

[8] K.H. Tan, Z.F. Huang. Structural responses of axially restrained steel beams with semirigid moment connection in fire. Journal of Structural Engineering, 2005;131:541-51.

[9] C.G. Bailey, I.W. Burgess, R.J. Plank. The lateral-torsional buckling of unrestrained steel beams in fire. Journal of Constructional Steel Research, 1996;36:101-19.

[10] A.S. Usmani, J.M. Rotter, S. Lamont, A.M. Sanad, M. Gillie. Fundamental principles of structural behavior under thermal effects. Fire Safety Journal, 2001;36:721-44.

[11] J.A. EI-Rimawi, I.W. Burgess, R.J. Plank. The influence of connection stiffness on the behavior of steel beams in fire. Journal of Constructional Steel Research, 1997;43:1-15.

[12] V.K.R. Kodur, M.M.S. Dwaikat. Effect of high temperature creep on the fire response of restrained steel beams. Materials and Structures, 2010;43:1327-41.

[13] D. Drysdale. An introduction to fire dynamics, 2rd edition. John Wiley and Sons. 1999.

[14] C. Zhang, G.Q. Li. Thermal response of steel columns exposed to localized fires - numerical simulation and comparison with experimental results. Journal of Structural Fire Engineering, 2011;2:311-7.

[15] C. Zhang, G.Q. Li. Thermal behavior of a steel beam exposed to a localized fire - numerical simulation and comparison with experimental results. In: Proceedings of the 4th International Conference on Protection of Structures against Hazards, Beijing, China, 2009, p. 409-15.

[16] Y. Hasemi, Y. Yokobayashi, T. Wakamatsu, A.V. Ptchelintsev. Modeling of heating mechanism and thermal response of structural components exposed to localized fires: A new application of diffusion flame modeling to fire safety engineering. NIST Internal Report 6030, National Institute of Standards and Technology, Gaithersburg, Maryland, 1997.

[17] Eurocode 1: Actions on structures - Part 1-2: General actions - Actions on structures exposed to fire. BSI, 2002.

[18] B.Y. Lattimer. Heat fluxes from fires to surfaces. In: SFPE Handbook of Fire Protection Engineering, 3rd edition, Section 2-4, Society of Fire Protection Engineers, Maryland, 2002.

[19] A.E. Jeffers, E.D. Sotelino. An efficient fiber element approach for the thermo-structural simulation of non-uniformly heated frames. Fire Safety Journal, 2012;51:18-26.

[20] V. Babrauskas. SFPE Handbbok of Fire Protection Engineering, 3rd edition, Section 3-1:Heat Release Rates, Society of Fire Protection Engineers, 2002.

[21] G.Q. Li, C. Zhang. Creep effect on buckling of axially restrained steel columns in real fires. Journal of Constructional Steel Research, 2012;71:182-8.

[22] A.H. Buchanan. Structural design for fire safety. John Wiley and Sons Ltd.; 2002

[23] Y. Yokobayashi, Y. Hasemi, Takashi. Wakamatsu, Takao. Wakamatsu. Heating mechanism of flat ceiling exposed to localized fire - An introduction to the fire safety design of building structures exposed to localized fire. J. Struct. Constr. Eng., AIJ, 1996;484:149-56. (in Japanese).

[24] Y. Yokobayashi, Y. Hasemi, Takashi. Wakamatsu, Takao. Wakamatsu. Experimental study on the heating mechanism and thermal response of a steel beam under ceiling exposed to localized fires. J. Struct. Constr. Eng., AIJ, 1997;498:169-75. (in Japanese).

[25] J. Myllymaki, M. Kokkala. Thermal exposure to a high welded I-beam above a pool fire. Proceedings of the 1st International Workshop on Structures in fire, Copenhagen, Denmark, 2000, p. 211-24.

[26] C. Zhang, G.Q. Li, Y.C. Wang. Sensitivity study on using different formulae for calculating the temperature of insulated steel members in natural fires. Fire Technology, 2012;48:343-66.

[27] G.Q. Li, C. Zhang. Thermal response to fire of uniformly insulated steel members: background and verification of the formulation reccomended by chinese code CECS200. Advanced Steel Construction, 2010;6:788-802.

[28] J.P. Holman. Heat transfer, 9th edition. McGraw-Hill Inc., 2002.

[29] J. Ding, G.Q. Li, Y. Sakumoto. Parametric Studies on Fire Resistance of Fire-resistant Steel Members, Journal of Constructional Steel Research, 2004;60:1007-27.

[30] T. T. Lie, B.A. Macaulay. Evaluation of the fire resistance of protected steel columns. Internal Report No. 583, National Research Concil Canada; 1989.

[31] BS 476-20. British Standard BS 476, Part 20: Method for determination of the fire resistance of load bearing elements of construction (General Principles), British Standard Institution. London, 1987.

Table 1: Investigated cases

Case	Beam	L	Restraints	LR	Fire type	Failure mode	T_{fail}
1a	B1	2000 mm	R&A	0.5	NFSC	buckling	720 ^{o}C
1b	B1	2000 mm	R&A	0.5	steady	buckling	777 ^{o}C
1c	B1	2000 mm	R&A	0.5	ISO834	buckling	676 ^{o}C
2a	B2	2000 mm	A	0.5	NFSC	buckling	687 ^{o}C
2b	B2	2000 mm	A	0.5	steady	deflection	744 ^{o}C
2c	B2	2000 mm	A	0.5	ISO834	deflection	649 ^{o}C
3a	B3	4500 mm	R&A	0.7	NFSC	buckling	798 ^{o}C
3b	B3	4500 mm	R&A	0.7	steady	buckling	798 ^{o}C
3c	B3	4500 mm	R&A	0.7	ISO834	deflection	703 ^{o}C
4a	B4	4500 mm	A	0.7	NFSC	buckling	454 ^{o}C
4b	B4	4500 mm	A	0.7	steady	buckling	474 ^{o}C
4c	B4	4500 mm	A	0.7	ISO834	deflection	514 ^{o}C

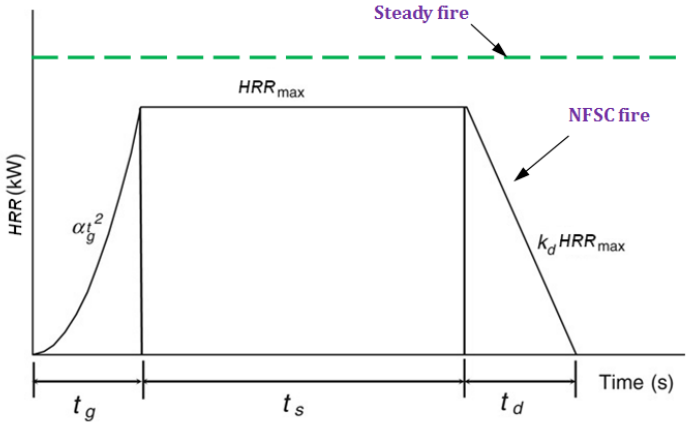

Figure 1: Illustration of the HRR history of a NFSC and steady fire

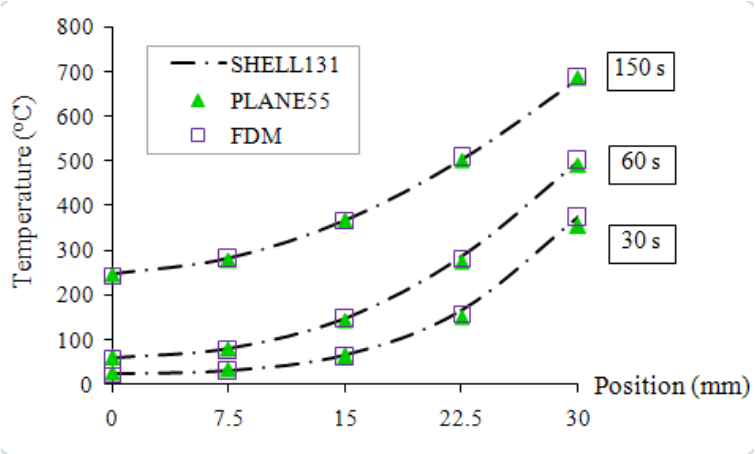

Figure 2: Comparison among the results of temperatures of a ceramic wall predicted by different methods

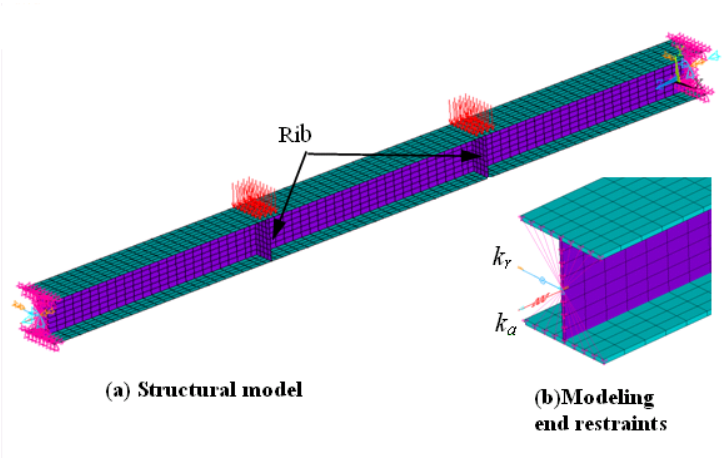

Figure 3: FE model of a restrained steel I beam in validation study for Li and Guo test [2]

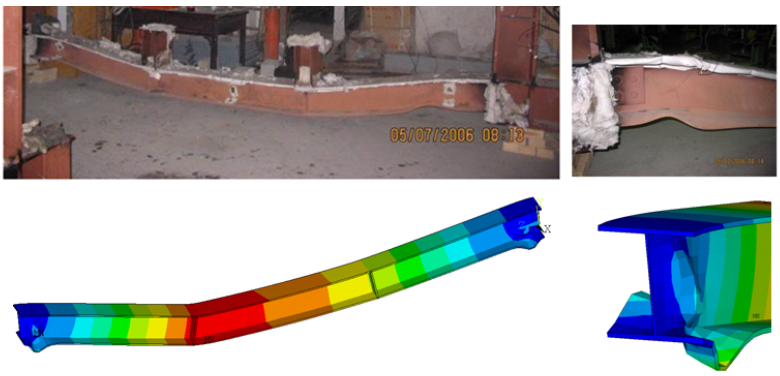

Figure 4: Numerical vs test results for Li and Guo test [2]

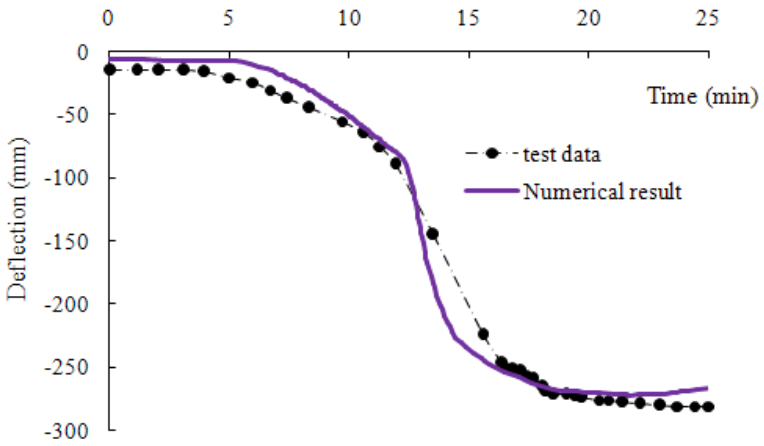

Figure 5: Predicted and measured deflection of the steel beam in [2]

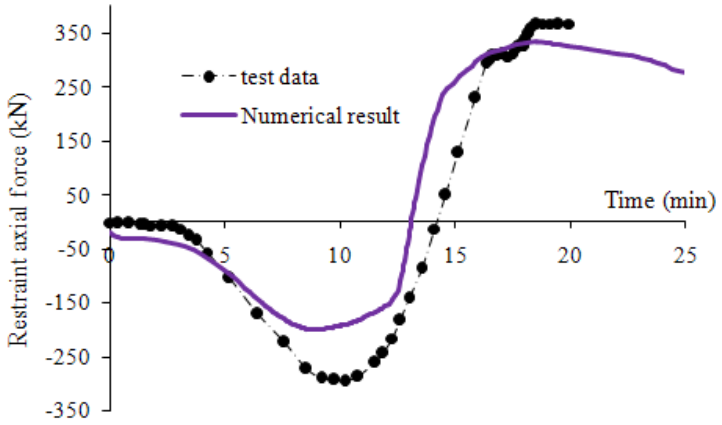

Figure 6: Predicted and measured restraint axial force of the steel beam in [2]

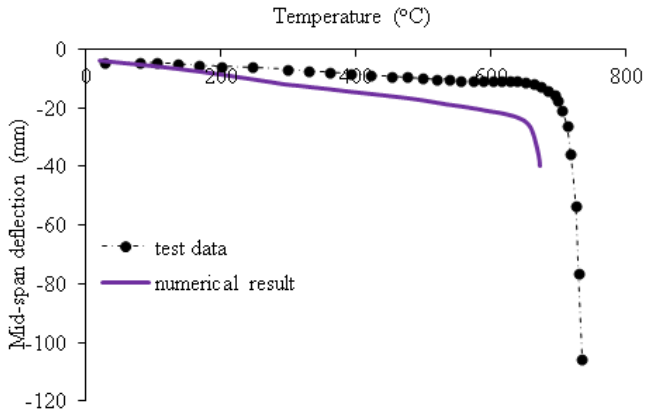

Figure 7: Predicted and measured deflection of the steel beam in [1]

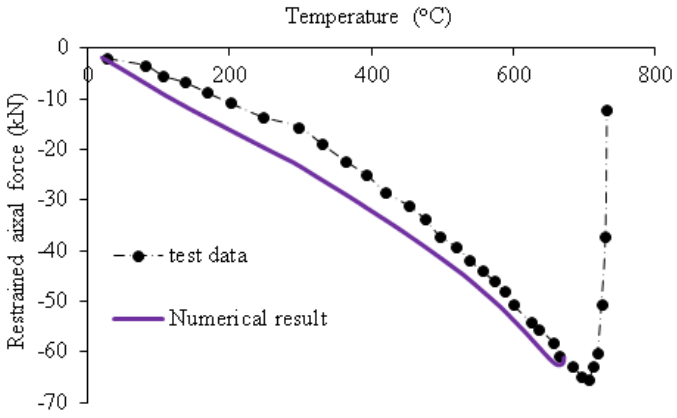

Figure 8: Predicted and measured restraint axial force of the steel beam in [1]

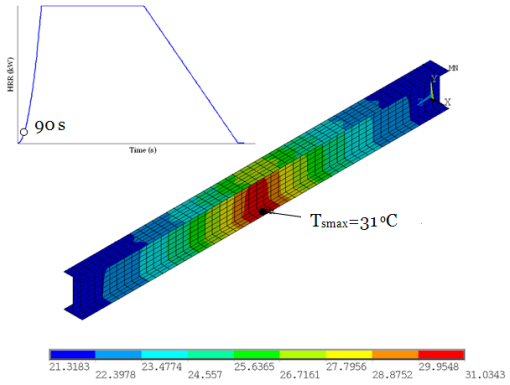

(a) Case 1, t=90 s

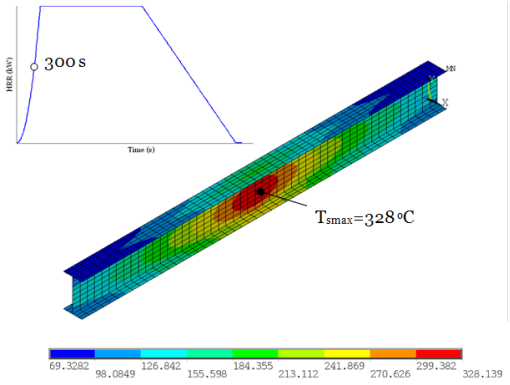

(b) Case 1, t=300 s

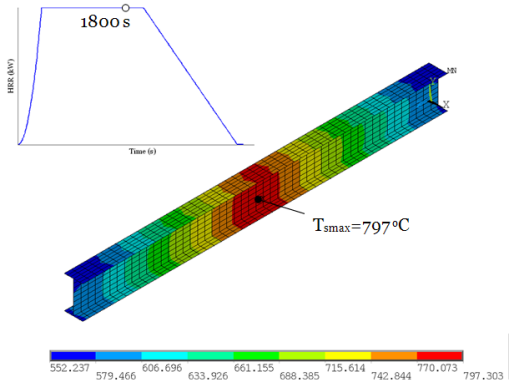

(c) Case 1, t=1800 s

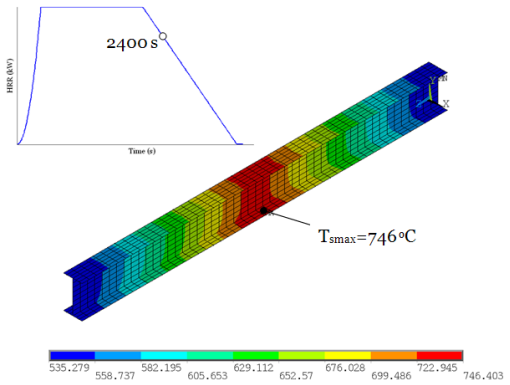

(d) Case 1, t=2400 s

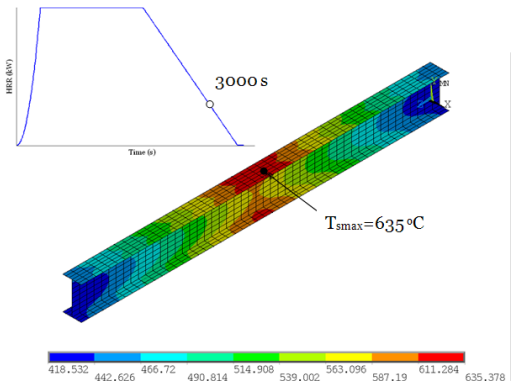

(e) Case 1, t=3000 s

Figure 9: Temperature results for steel beam subjected to NFSC fire

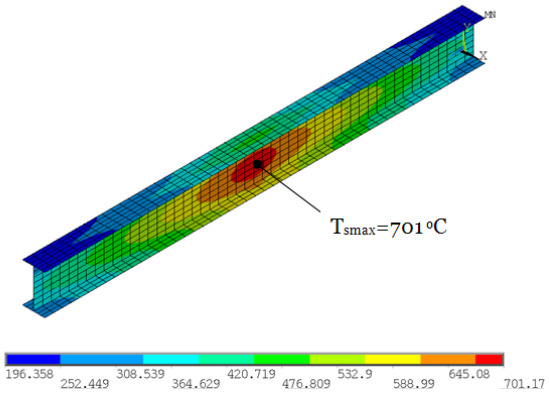

(a) Case 1, t=300 s

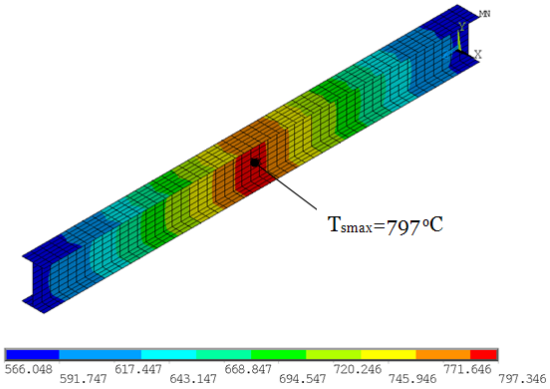

(b) Case 1, t=3000 s

Figure 10: Temperature results for steel beam subjected to STEADY fire

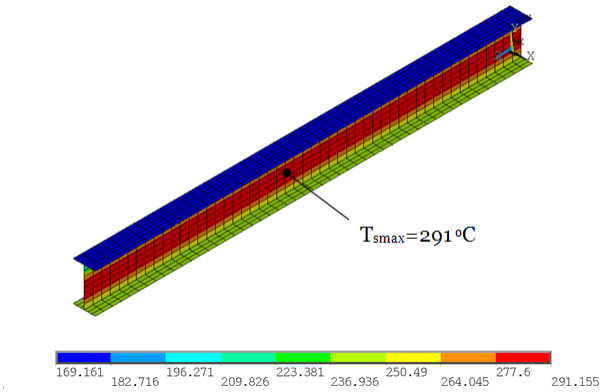

(a) Case 1, t=300 s

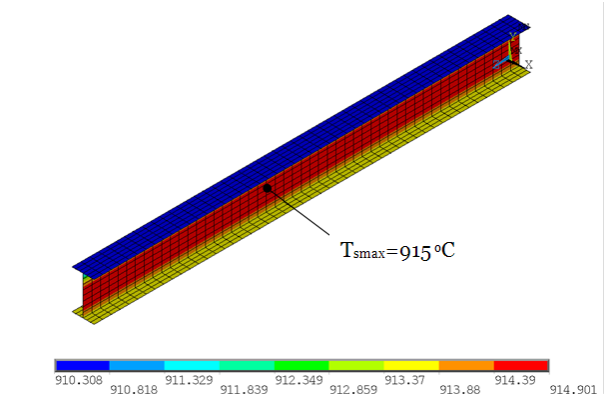

(b) Case 1, t=3000 s

Figure 11: Temperature results for steel beam subjected to ISO834 fire

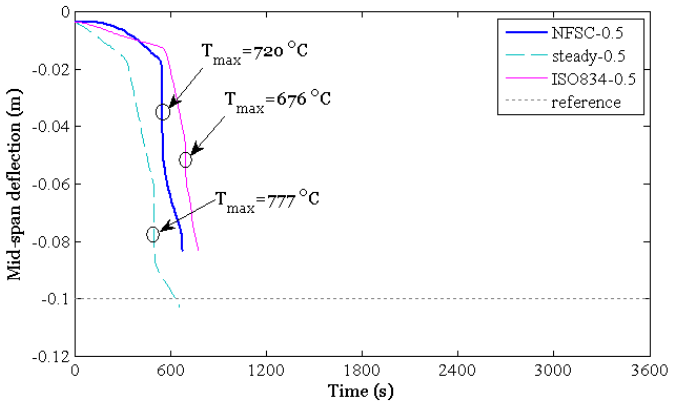

(a) Deflection

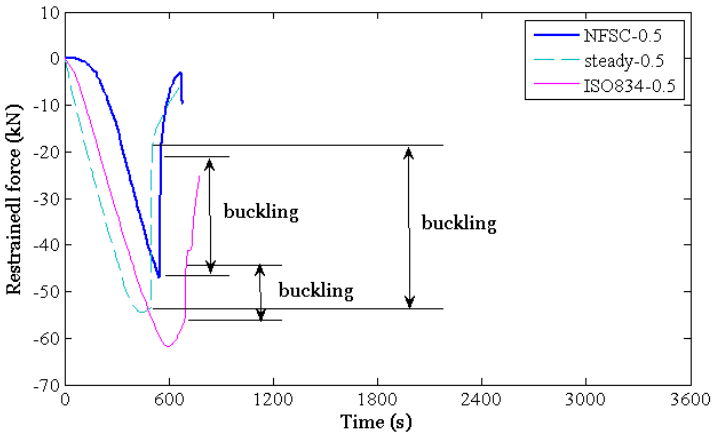

(b) Force

Figure 12: Results for mid-span deflection and reaction force for restrained steel beam B1 in different fires

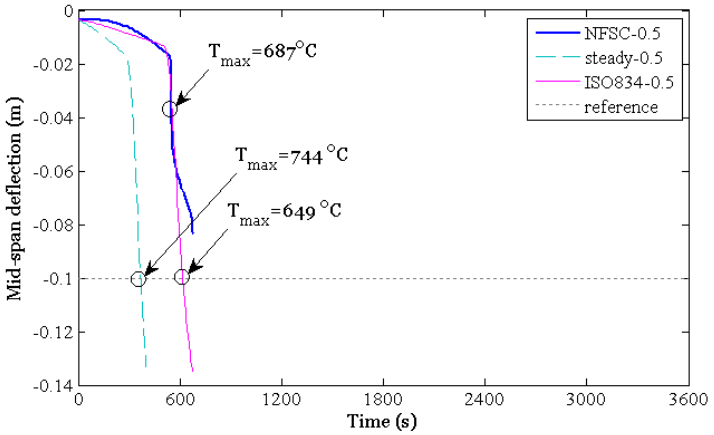

(a) Deflection

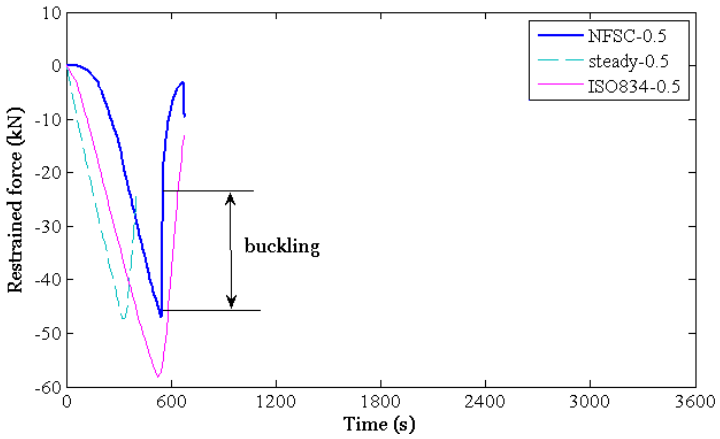

(b) Force

Figure 13: Results for mid-span deflection and reaction force for restrained steel beam B2 in different fires

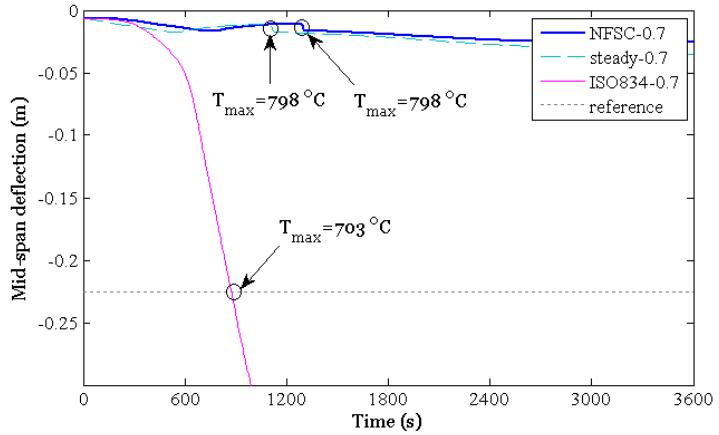

(a) Deflection

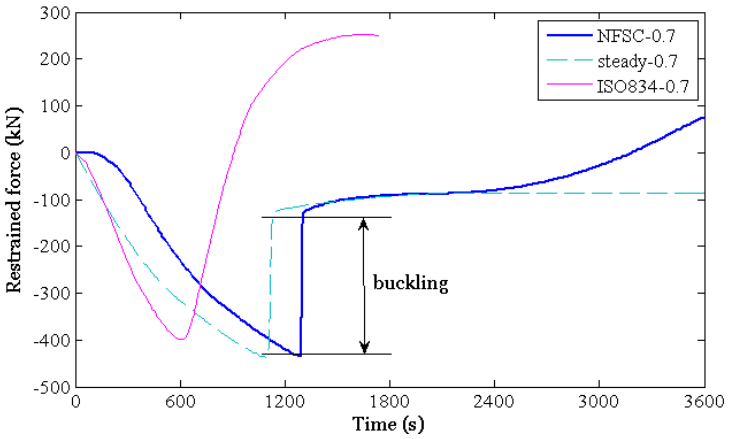

(b) Force

Figure 14: Results for mid-span deflection and reaction force for restrained steel beam B3 in different fires

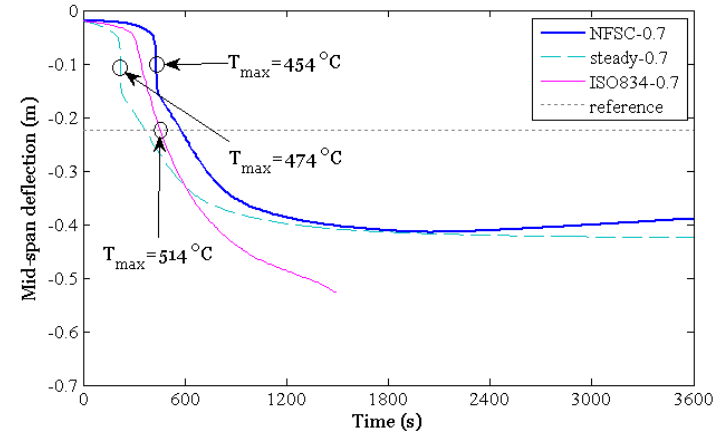

(a) Deflection

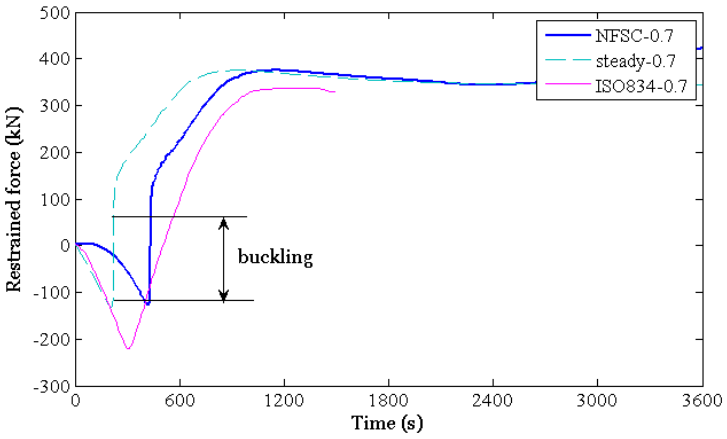

(b) Force

Figure 15: Results for mid-span deflection and reaction force for restrained steel beam B4 in different fires

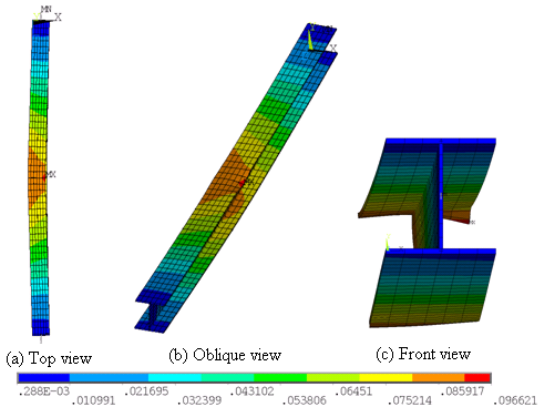

Figure 16: Results for deformation for beam B4 in NFSC fire

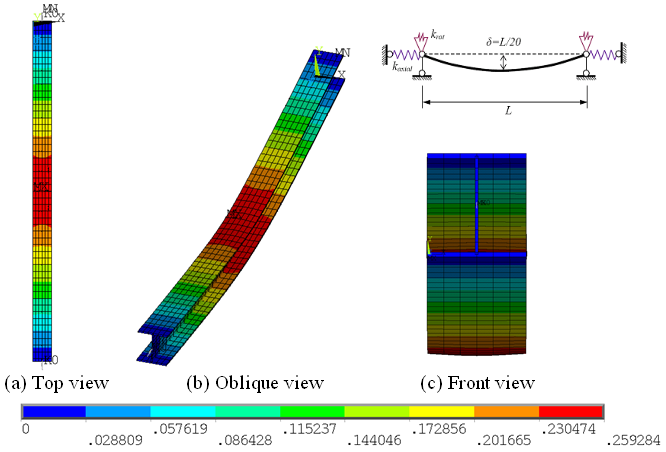

Figure 17: Results for deformation for beam B4 in ISO834 fire